Biochar as a Fuel: 4. Emission Behavior and Characteristics of PM1 and PM10 from the Combustion of Pulverized Biochar in a Drop-Tube Furnace

ARTICLE *in* ENERGY & FUELS · MAY 2011

Impact Factor: 2.79 · DOI: 10.1021/ef200296u

2 AUTHORS:

Xiangpeng Gao
Curtin University
30 PUBLICATIONS **319** CITATIONS
SEE PROFILE

Hongwei Wu
Yale University
91 PUBLICATIONS **2,402** CITATIONS
SEE PROFILE

energy&fuels

ARTICLE

pubs.acs.org/EF

Biochar as a Fuel: 4. Emission Behavior and Characteristics of PM_1 and PM_{10} from the Combustion of Pulverized Biochar in a Drop-Tube Furnace

Xiangpeng Gao and Hongwei Wu*

Fuels and Energy Technology Institute, Department of Chemical Engineering, Curtin University of Technology, GPO Box U1987, Perth, Western Australia 6845, Australia

ABSTRACT: Six biochar samples were produced from both slow and fast pyrolysis of mallee bark at 400−550 °C, respectively; such temperatures are typically used for biochar and/or bio-oil production in practice. Under the pyrolysis conditions, the biochar yields range from 26.7 to 37.0% and the majority (78.5−100.0%) of alkali and alkaline earth metallic (AAEM) species (mainly Na, K, Mg, and Ca) in biomass are retained in the biochars, while the retention of Cl in biochars is only 2.0−33.4%. The raw biomass and its derived biochar samples were then combusted in a laboratory-scale drop-tube furnace (DTF) at 1300 °C to investigate the emission behavior and characteristics of sub-micrometer particulate matter (PM_1) and PM with an aerodynamic diameter less than 10.0 μm (PM_{10}). The particle size distribution (PSD) of PM_{10} from raw biomass combustion has a bimodal size distribution, while the PSDs of PM_{10} from biochar combustion generally show a unimodal distribution. Although most inorganic species are retained in the biochar during pyrolysis, it is interesting to note that the combustion of biochars leads to a substantial reduction in the emission of PM_1 (and the mass of Na, K, and Cl in PM_1) that dominantly consists of PM with a size less than 0.1 μm ($PM_{0.1}$) in comparison to biomass combustion, apparently because of the removal of volatiles and Cl from the raw biomass during pyrolysis for biochar preparation. The results imply that the combustion of volatiles (including the released inorganic species), which is particularly important during biomass combustion, is mainly responsible for PM_1 emission. Meanwhile, considerable increases in the emission of coarser particulate matter with an aerodynamic diameter between 1 and 10 μm (PM_{1-10}) and the mass of Mg and Ca in PM_{1-10} are also evident during biochar combustion, most likely as a result of more porous structure and increased ash loading of biochars.

1. INTRODUCTION

Mallee biomass is an important second-generation renewable feedstock for the future energy security and sustainable development in rural and regional Australia. It is a byproduct of the dryland salinity management of premium agriculture land and enhances (rather than competes with) food production.[1,2] The production of mallee biomass is on a large scale and economic and has small carbon and energy footprints.[1,3−5] However, the major hurdles that limit the use of biomass as fuel are the bulky nature, high moisture content, high transport cost, and poor grindability of the biomass.[6−10]

Because biomass is typically produced/available in rural and regional areas, an attractive use strategy to address aforementioned issues is to deploy distributed pyrolysis as a flexible technology[11−15] to convert the bulky raw biomass locally into high-energy-density fuels, such as bio-oil[12,13,16,17] and/or biochar.[15,18,19] While bio-oil can be transported to centralized plants and has the potential for further upgrading and refining to produce liquid transport fuels,[12,13,20] biochar as a solid fuel has superb fuel properties, good grindability, and high energy density and, therefore, is suitable for applications such as gasification and combustion, as well as co-firing in coal-based power stations.[18,19,21]

Direct biomass combustion or co-firing biomass with coal are matured technologies[6−10] for power generation and promising short-term solutions for reducing CO_2 emission from power generation. However, biomass combustion/co-firing contributes significantly to the fine particulate matter (PM) emission,[22−30] especially sub-micrometer PM (PM_1), which is easy to escape from dust cleaning equipment.[31,32] Biochar also contains abundant inherent inorganic species[21,33,34] that may potentially lead to significant PM emission. However, while the emission behavior of PM_1 and PM_{10} (PM with an aerodynamic diameter less than 10.0 μm) from raw biomass combustion were investigated previously,[28,35,36] little work has been performed thus far on PM_{10} emission from biochar combustion.

Therefore, a good understanding on the emission behavior and characteristics of PM_1 and PM_{10} from biochar combustion is important to practically use biochar as a fuel in direct combustion or co-firing applications. The key objective of this study is therefore to carry out a systematic investigation on the properties of PM_1 and PM_{10} emitted from the combustion of biochars (produced from biomass pyrolysis under controlled conditions relevant to practical biochar production) in a laboratory-scale drop-tube furnace (DTF) system. This study continues our series of work on biochar as a fuel, including part 1 (10.1021/ef900494t)[18] on biochar fuel chemistry and grindability, part 2 (10.1021/ef901435f)[19] on the significant differences in biochars produced from various mallee biomass components, and part 3 (10.1021/ef101472f)[37] on biochar thermal annealing at mild temperatures.

Received: February 24, 2011
Revised: May 6, 2011
Published: May 18, 2011

Table 1. Properties of Raw Biomass and Its Derived Biochars Used in This Study (SH-Char-xxx, Biochar Prepared from the Slow Heating Pyrolysis of Biomass at xxx °C; FH-Char-xxx, Biochar Prepared from the Fast Heating Pyrolysis of Biomass at xxx °C)

samples	raw biomass	SH-Char-400	SH-Char-450	SH-Char-500	SH-Char-550	FH-Char-400	FH-Char-500
			Proximate Analysis				
moisture (% ad)	5.6	5.8	4.0	4.4	3.1	5.1	4.6
ash (% db)	4.0	9.0	10.8	11.3	12.0	10.3	13.7
VM[a] (% db)	74.2	34.1	26.6	24.3	19.3	39.6	31.9
FC[b] (% db)	21.8	56.9	62.6	64.4	68.7	50.1	54.4
			Ultimate Analysis (% daf)				
C	51.02	74.95	82.85	85.12	88.98	72.07	80.18
H	5.61	3.61	3.25	2.92	2.39	3.77	3.22
N	0.26	0.51	0.56	0.66	0.64	0.63	0.66
S	0.02	0.04	0.02	0.03	0.02	0.04	0.06
Cl	0.17	0.02	0.01	0.02	0.01	0.07	0.24
O[c]	42.92	20.87	13.31	11.25	7.96	23.42	15.64
lower heating value (LHV) (MJ/kg, ad)	17.2	24.1	25.7	26.1	27.4	23.6	23.4
			Inorganic Species Content (% db)				
Na[d]	0.2550	0.6360	0.7465	0.7424	0.8477	0.7082	0.9677
K[d]	0.1407	0.3108	0.3238	0.3668	0.3704	0.3472	0.4236
Mg[d]	0.0869	0.2118	0.2450	0.2333	0.2721	0.2179	0.3187
Ca[d]	1.3937	3.6168	3.8316	4.2265	4.1750	3.9313	5.5712
Al[e]	0.0017	0.0077	0.0062	0.0047	0.0053	0.0059	0.0132
Si[e]	0.0021	0.0102	0.0149	0.0196	0.0134	0.0071	0.0108
Fe[e]	0.0016	0.0182	0.0120	0.0057	0.0049	0.0041	0.0103
P[e]	0.0257	0.0626	0.0672	0.0717	0.0722	0.0726	0.1086

[a] Volatile matter. [b] Fixed carbon. [c] By difference. [d] Analyzed by IC. [e] Analyzed by ICP−AES.

2. EXPERIMENTAL SECTION

2.1. Preparation and Characterization of Raw Biomass and Biochar Samples. The bark component was separated from a batch of green mallee trees (*Eucalyptus loxophleba* ssp. *lissophloia*) harvested from Narrogin, Western Australia, Australia. A raw biomass sample was then prepared by drying the bark at 40 °C in a large lab oven, cutting, milling, and then sieving the sample into the size fraction of 75−150 μm for experiments. It should be noted that the batch of the bark sample is different from the ones used in our previous study.[38]

Biochar samples were prepared from the pyrolysis of the raw biomass sample using a quartz drop-tube/fixed-bed reactor. The detailed description of the reactor system can be found elsewhere.[21,39] Pyrolysis experiments were carried out at 400−550 °C using argon (UHP 99.999%, 2.0 L min^{-1}) as a carrier gas. The reactor can be used for pyrolysis experiments at both slow- and fast-heating rates. For pyrolysis experiments at a slow-heating rate, the sample was first loaded into the reactor that was then heated from ambient to the desired pyrolysis temperature at 10 K min^{-1} with a further holding of 30 min. For pyrolysis experiments at a fast-heating rate, the reactor has the features of both a drop-tube reactor and a fixed-bed reactor. The reactor was first preheated to the desired pyrolysis temperature. The biomass particles were then fed into the reactor at a low feeding rate (∼0.1 g min^{-1}) via a feeder. Once the biomass particles were injected into the hot reactor zone, rapid pyrolysis took place (similar to a normal drop-tube reactor). However, different from a normal drop-tube reactor, the char particles formed in this reactor system after pyrolysis remained on the frit of the reactor, while volatiles were swept away. Once a pyrolysis experiment (at a slow- or fast-heating rate) was completed, the reactor was lifted out of the furnace immediately and cooled naturally with argon continuously flowing through the reactor. Hereafter, in this paper, the biochar samples produced from slow pyrolysis at 400, 450, 500, and 550 °C are referred to as "SH-Char-400", "SH-Char-450", "SH-Char-500", and "SH-Char-550", while those produced from fast pyrolysis at 400 and 500 °C are referred to as "FH-Char-400" and "FH-Char-500".

Fast pyrolysis experiments at 1300 °C were carried out for the raw biomass, "SH-Char-400", "SH-Char-500", "FH-Char-400", and "FH-Char-500" in a lab-scale DTF system using argon as a carrier gas, to investigate the structure change of chars produced from the fast pyrolysis of these fuels at 1300 °C. A total gas flow rate of 5.6 L min^{-1} argon passed through the reactor in two streams: a primary stream of argon (1 L min^{-1}) via the feeder and a secondary stream of argon (4.6 L min^{-1}) via the reactor inlet. The detailed description and operation procedure of the DTF system can be found elsewhere.[38] A fuel feeding rate of ∼0.05 g min^{-1} was used. Hereafter, the char samples produced from the fast pyrolysis of raw biomass, "SH-Char-400", "SH-Char-500", "FH-Char-400", and "FH-Char-500" at 1300 °C are denoted as "Char-1300-raw biomass", "Char-1300-SH-Char-400", "Char-1300-SH-Char-500", "Char-1300-FH-Char-400", and "Char-1300-FH-Char-500", respectively.

The calorific values of raw biomass and its derived biochars produced from slow and fast pyrolysis at 400−550 °C were measured using a Leco AC-350 analyzer. The micropore surface area of the chars produced from fast pyrolysis at 1300 °C was determined via CO_2 adsorption analyzed by the Dubinin−Astakhov equation. The biomass and biochar samples were also ashed, acid-digested, and then quantified by ion chromatography (IC) and/or inductively coupled plasma−atomic emission spectroscopy (ICP−AES), following a purposely designed procedure detailed elsewhere.[38] The fuel properties of raw biomass and its derived biochars and also the contents of inorganic species in raw biomass and biochar samples are summarized in Table 1. It can be seen that the inorganic species in these fuels are dominantly alkali and alkaline

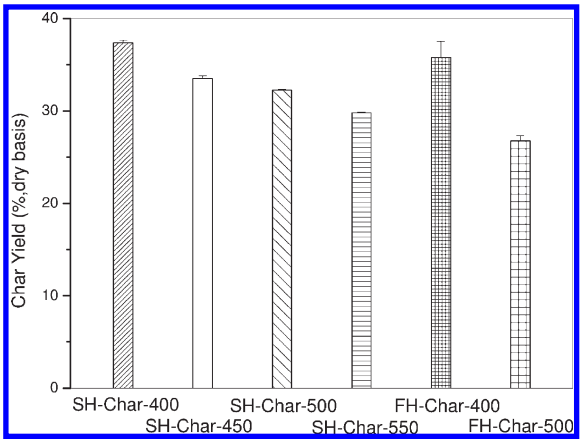

Figure 1. Biochar yields from the pyrolysis of raw biomass under various conditions.

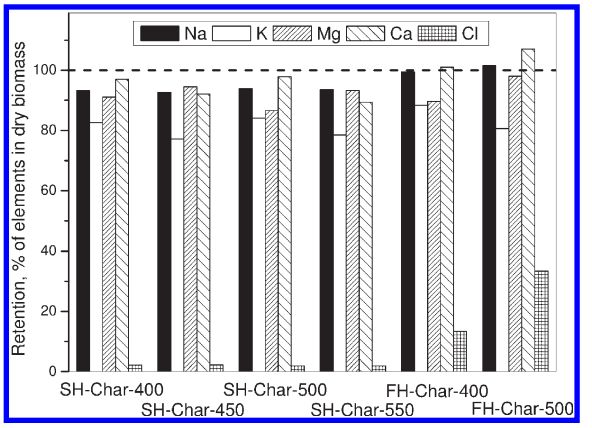

Figure 2. Retentions of AAEM species and Cl in biochars produced from the pyrolysis of raw biomass at different conditions.

earth metallic (AAEM) species and Cl, with very low contents of Al and Si. It should be noted that the S contents in both raw biomass and biochars are also very low, with an extremely low S/Cl ratio of 0.1 in raw biomass. The sulfation effect of S plays an insignificant role because a much higher S/Cl ratio (from 4.7 to 7.5) is required to cause significant sulfation reactions during biomass combustion.[40] Therefore, such unique features of the fuel samples simplify the study because the chemical composition analysis can be focused on AAEM species and Cl.

2.2. Combustion Experiments, PM Sampling, and Analysis Methods. The combustion experiments were carried out in the same DTF system that was used in our previous study.[38] In this study, the furnace temperature was kept at 1300 °C. During combustion, the primary and secondary air flow rates were 1.0 and 4.6 L min^{-1}, respectively. The fuel feeding rate was ~0.05 g min^{-1}. The value of λ (expressed as the ratio of the actual air/fuel ratio to the stoichiometric air/fuel ratio) was ~26. The residence time of pulverized fuel particles in the isothermal zone of the DTF was estimated as ~1.7 s. In all experiments, the flue gas temperature at the outlet of the sampling probe was adjusted at 115 °C and complete combustion was achieved. The sampling of PM in the combustion flue gas followed a procedure described elsewhere.[38] Briefly, the PM_{10}-containing flue gas (after dilution, PM_{10} concentration < 30 mg/Nm^3) was separated by the cyclone to remove the coarse ash particles (aerodynamic diameter of >10 μm) and then directed to a Dekati low-pressure impactor (DLPI) and its backup filter for size-segregated collection (<10 μm). The sampling system (including diluter, cyclone, DLPI, and the sampling lines) was kept at 115 °C, a temperature the same as that of the flue gas at the sampling probe exit, to avoid possible acid gas condensation and suppress particle coagulation during the sampling process.[38] It is important to note that it is impossible to achieve an elemental mass balance for ash-forming species in fuel and combustion products because part of the combustion products may react with the furnace wall. Therefore, this study focused on the emission behavior and characteristics of PM. The mass-based particle size distribution (PSD) was obtained by measuring the mass of PM collected in each stage of DLPI using a Mettler MX5 microbalance (accuracy of 0.001 mg). The collected PM samples were also subject to chemical composition analysis. Duplicated batches of samples were prepared, one for the analysis of AAEM species and the other for the analysis of Cl, following a procedure described elsewhere.[38]

3. RESULTS AND DISCUSSION

3.1. Biochar Yields and the Retention of AAEM Species and Cl in Biochars. Figure 1 shows the biochar yields from pyrolysis of raw biomass at various conditions on a dry basis. As expected, at a given pyrolysis temperature, a higher biochar yield is obtained in slow pyrolysis in comparison to that of fast pyrolysis. A higher pyrolysis temperature also leads to a lower biochar yield, in either slow or fast pyrolysis of biomass. Therefore, "SH-Char-400" (i.e., the biochar produced from slow pyrolysis at 400 °C) has the highest biochar yield of ~37.0%, while the "FH-Char-500" (i.e., the biochar produced from fast pyrolysis at 500 °C) has the lowest yield of ~26.7%.

Figure 2 further shows the retention of AAEM species and Cl in the biochars after biomass pyrolysis under various conditions. It is clear that, after pyrolysis, the majority of the AAEM species in biomass have been retained in the biochars, with retentions of AAEM species around 78.5−100.0%. This is also expected given the low pyrolysis temperatures (400−550 °C). Even at such low temperatures, a small proportion of AAEM species was volatilized. Such a phenomenon is known to be possible because of the volatilization of AAEM species along with the release of carboxylate structures during pyrolysis, as observed in previous studies.[41,42] Ca has the highest retention of around 92.2−100.0%, while K appears to have the lowest retention of around 78.5−88.3%. Contrary to AAEM species, the majority of Cl was volatilized at such low temperatures as 400−550 °C during the pyrolysis of raw biomass, with retentions of around 2.0−33.4%. Such a significant release of Cl at low temperatures of 400−550 °C during biomass pyrolysis was also observed in previous studies.[43,44] It is also interesting to note that the retentions of Cl in fast pyrolysis are higher than those of slow pyrolysis. Particularly, for fast pyrolysis at 500 °C, Cl retention is ~33.4%, possibly because of the strong interactions between Cl and char matrix during pyrolysis.[45]

3.2. PM_1 and PM_{10} Yields during the Combustion of Biomass and Biochars. Figure 3 presents the data on PM_{10} yields from the combustion of the raw biomass and its derived biochars. For meaningful comparisons, it is important to note that the PM_{10} yields are normalized to three different bases (i.e., equivalent biomass, ash, and energy input) and presented in panels a and b, c and d, and e and f of Figure 3, respectively.

Panels a and b of Figure 3 present the PM_1 and PM_{10} emission data normalized to the equivalent amount of starting raw biomass (db), enabling us to provide insight into the effect of pyrolysis as a technology for biomass pretreatment (i.e., for biochar production) on PM emission during biomass/biochar combustion. It is interesting to note that, at an equivalent amount of raw biomass, the PM_1 yields from the combustion of biochars are

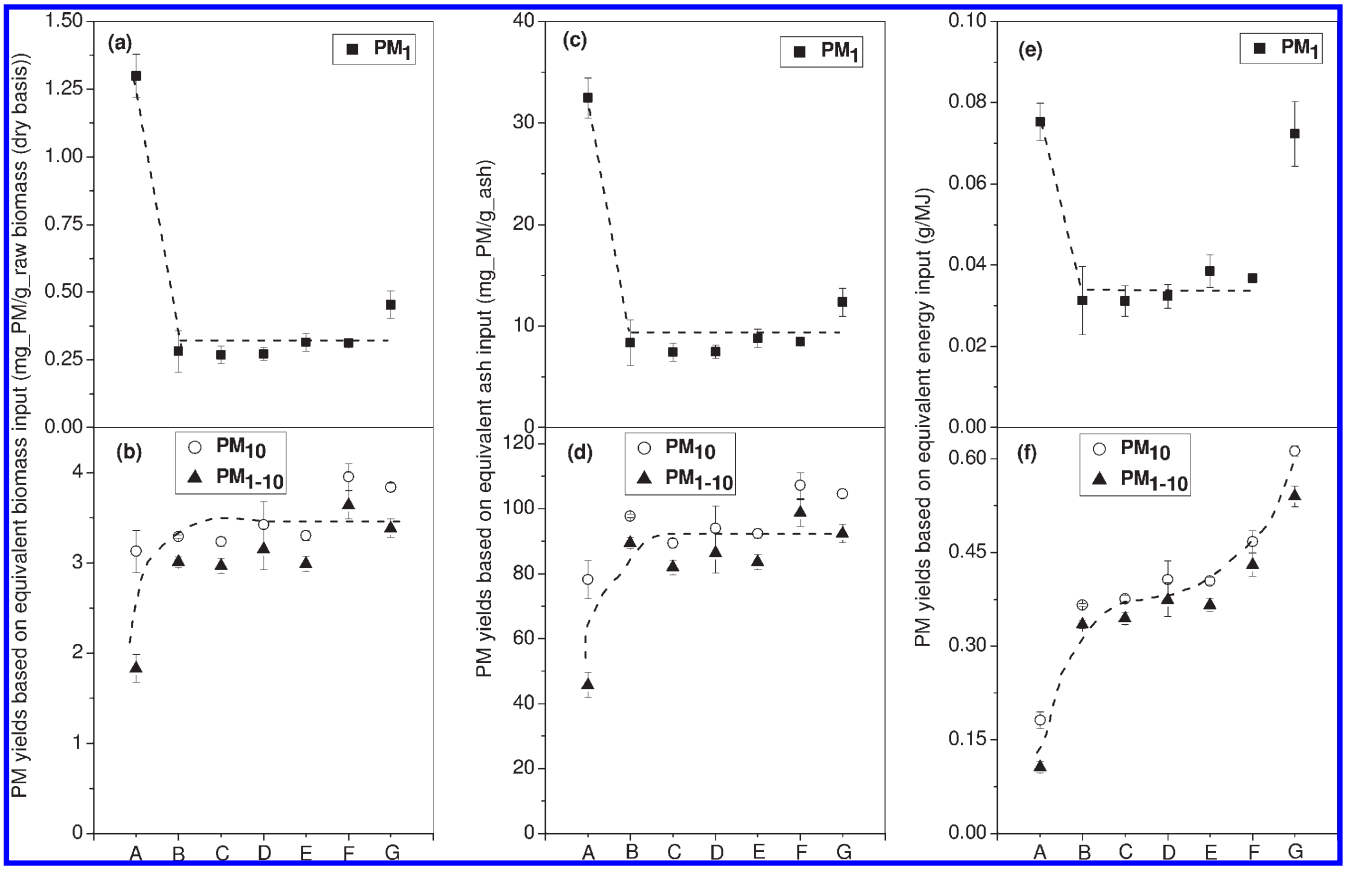

Figure 3. PM yields from raw biomass and biochars combustion: (a) PM_1 and (b) PM_{10} yields, normalized to equivalent biomass (db) input into the furnace; (c) PM_1 and (d) PM_{10} yields, normalized to equivalent ash input into the furnace; and (e) PM_1 and (f) PM_{10} yield, normalized to equivalent energy input into the furnace. Equivalent biomass input is calculated from the char yields and the mass of biochars fed into the DTF. Equivalent ash input is calculated from the mass of fuel (db) fed into furnace and its ash content (wt%, db). Equivalent energy input is calculated from the LHV of raw biomass and biochars and their mass (db) fed into the DTF. X-axis labels: A, Raw Biomass; B, SH-Char-400; C, SH-Char-450; D, SH-Char-500; E, SH-Char-550; F, FH-Char-400; and G, FH-Char-500.

substantially lower than that from direct raw biomass combustion (see Figure 3a). Clearly, the use of biochars from the biomass pyrolysis in fuel applications may lead to substantial reduction in PM_1 emission, likely related to the removal of volatiles (including the released inorganic species). One exception is in the case of fast-heating char at 500 °C; the PM_1 yield is higher than other chars, implying that fuel properties may also play an important role. On the contrary, the PM_{10} yields from the combustion of biochars are higher than that from direct biomass combustion (see Figure 3b). As the PM_1 yields during biochar combustion are reduced, such significant increases in PM_{10} yields are clearly due to the increase in the yields of coarser particulates with an aerodynamic diameter between 1 and 10 μm (PM_{1-10}) during biochar combustion. Because super-micrometer PM is generally produced from char fragmentation during combustion, the results also seem to suggest that the pretreatment of the fuel via pyrolysis also leads to a significant enhancement of char fragmentation during combustion.

After low-temperature pyrolysis, the ash content of the fuel is increased substantially from 4.0% db for biomass to 9.0−13.7% db for biochars depending upon pyrolysis conditions (see Table 1). Therefore, the PM_{10} yields during a fuel combustion normalized to fuel ash content will further provide some plausible indication on the ability of the unit mass of ash-forming species in the fuel for PM emission. Such data are presented in panels c and d of Figure 3. It is not surprising that, in this case, the shapes of panels c and d of Figure 3 are similar to those of panels a and b of Figure 3, because the majority of ash-forming elements, such as AAEM species, were retained in biochars after low-temperature biomass pyrolysis (see Figure 2). Clearly, in comparison to those in the biomass, the ash-forming species in the biochar has a much poorer ability in PM_1 emission but a significantly enhanced ability in PM_{1-10} emission.

The substantial reductions in PM_1 yields during biochar combustion based on an equivalent biomass mass and unit ash input, respectively, are important findings. Such data demonstrate another good feature of using biochar as a fuel, in addition to its high energy density, good grindability, and good fuel properties for better matching with coal in co-firing application.[18,19] The data normalized to equivalent energy input into the furnace will be discussed in section 3.5.

3.3. Mass-Based and Elemental-Mass-Based PSDs of PM_{10}. To further understand the characteristics of PM_{10} emission during the combustion of biomass and biochars, analyses were performed to obtain the data on mass-based and elemental-mass-based PSDs of PM_{10}. The data on mass-based and elemental-mass-based PSDs of PM_{10} are plotted in Figures 4 and 5, respectively.

As shown in Figure 4, the mass-based PSD of PM_{10} collected from raw biomass combustion normalized to equivalent raw biomass has a bimodal size distribution, i.e., a fine mode with a mode diameter of ~0.022 μm and a coarse mode with a mode

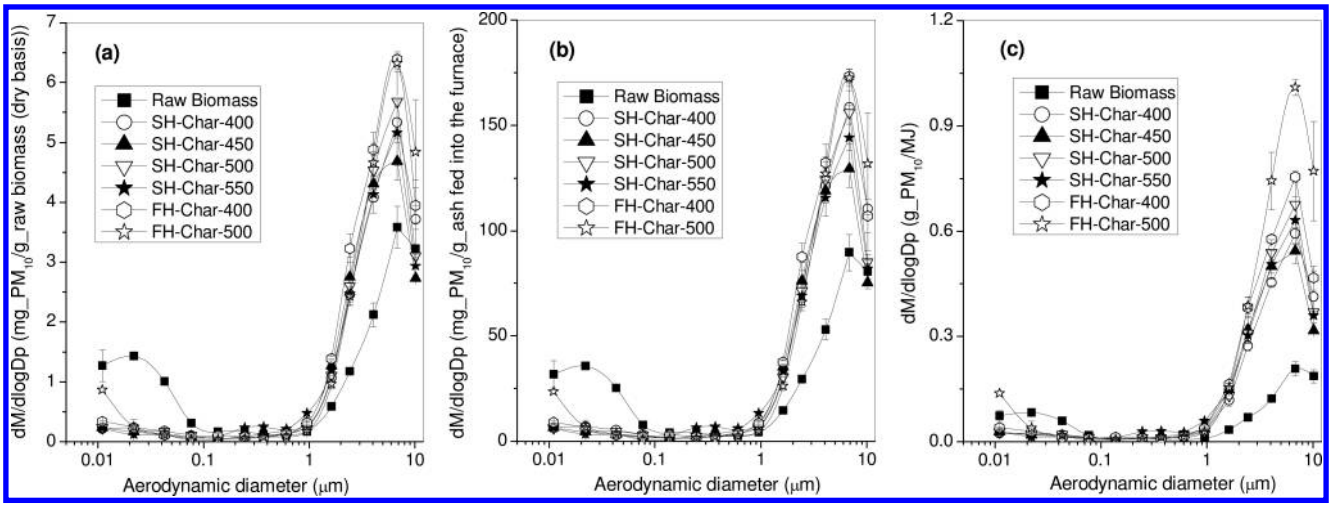

Figure 4. PSD of PM_{10} from the combustion of raw biomass and biochars: (a) graphs normalized to equivalent biomass (db) input into the furnace, (b) graphs normalized to equivalent ash input into the furnace, and (c) graphs normalized to equivalent energy (LHV) input into the furnace.

diameter of ~6.8 μm. However, the PSDs of PM_{10} from biochar combustion generally show a unimodal distribution with only a coarse mode of ~6.8 μm. The fine mode generally disappears in PM_{10} produced from biochar combustion, leading to significantly low PM_1 yields, as shown in Figure 3. The only exception is the PSD of PM_{10} from "FH-Char-500" combustion, which also shows a fine mode with a mode diameter of less than ~0.022 μm, possibly because of the high Cl content of the biochar, as discussed in the next section. Furthermore, the data on the mass-based PSDs of PM_{10} in Figure 4 clearly show that significant PM_1 generated from biomass combustion dominantly contains PM with a size less than 0.1 μm ($PM_{0.1}$). It is clear that the significant reductions in PM_1 emission during biochar combustion are due to the very low $PM_{0.1}$ yields for all biochar samples (see panels a and c of Figure 3 and panels a and b of Figure 4).

Furthermore, the data on elemental mass size distributions of PM_{10} normalized to the unit mass of equivalent raw biomass (db) further show that Na, K, and Cl also generally have a unimodal distribution from the combustion of both raw biomass and biochars (see Figure 5). Na, K, and Cl are dominantly contained in PM_1 (more precisely $PM_{0.1}$) in a single mode with a mode diameter of ~0.022 μm, which is the same as the mode diameter of the fine mode in the mass-based PSDs of PM_{10} (see Figure 4). The data on the elemental yields of AAEM species and Cl (see Figure 6) further demonstrate that the dominant presence of Na, K, and Cl in PM_1 is most likely due to the known mechanisms, such as homogeneous nucleation and/or heterogeneous condensation, of the Na-, K-, and Cl-containing vapors on fine particulates.[22,23,36,46,47]

Additionally, the data in Figure 5 also show that Mg and Ca also have a unimodal distribution in PM_{10} from the combustion of both raw biomass and biochars. However, Mg and Ca are concentrated in PM_{1-10} in a single mode with a mode diameter of ~6.8 μm, which is also the same as the coarse mode in the mass-based PSDs of PM_{10} (see Figure 4). The data in Figure 6 clearly show that PM_{1-10} is mainly produced from the refractory elements (Mg and Ca) in the burning char particles, in agreement with previous studies[22,23,36,46] and our recent related work.[38]

Not only the PM_1 yield (see Figures 3 and 4) but also the mass of Na, K, and Cl, which are dominantly contained in PM_1, are substantially reduced during biochar combustion in comparison to those from raw biomass combustion (see panels a−c and f−h of Figure 5). Because Na, K, and Cl are dominantly contained in $PM_{0.1}$, such particle mass and element (Na, K, and Cl) mass reductions in PM_1 mainly take place in the ultrafine particles ($PM_{0.1}$). Oppositely, the data in Figure 4 demonstrate a substantial increase in the mass of PM in the size range of 1.6−10.2 μm (with a mode diameter of 6.8 μm) from biochar combustion in comparison to that from raw biomass combustion. As shown in panels d and e and i and j of Figure 5, such increases in the coarse PM yields are due to the substantial increases in the mass of Mg and Ca in PM_{1-10} within the size range of 1.6−10.2 μm.

3.4. Further Discussion. Considering the data in sections 3.1−3.3 together, the possible mechanisms responsible for the significant discrepancies in the emission characteristics of PM_1 and PM_{10} from the combustion of raw biomass and biochars may be deduced. A key difference between biomass and biochars as fuels is the removal of volatiles (including released inorganic species) during biomass low-temperature (400−550 °C) pyrolysis for biochar production. Furthermore, it should be noted that, during biomass pyrolysis for biochar preparation, the majority of the AAEM species (78.5−100.0%) is retained in biochars (see Figure 2). However, the AAEM species retained in the biochars, although in substantial amounts, are not responsible for the significantly higher $PM_{0.1}$ yield during the combustion of raw biomass, because the contribution of biochar combustion to the $PM_{0.1}$ yield is limited (see panels a and b of Figure 4). In other words, the combustion of volatiles (including the released inorganic species) seems to be the dominant mechanism for $PM_{0.1}$ formation, although there are only small proportions (7−20%) of Na and K released with volatiles during pyrolysis (see Figure 2). Therefore, the significant reductions in PM_1 (or $PM_{0.1}$) yields and the mass yields of Na, K, and Cl (dominantly contained in $PM_{0.1}$) from biochar combustion in comparison to those from raw biomass combustion (see Figures 3−6) are most likely due to the lack of the contribution of volatile (including the released inorganic species) combustion to PM_1 formation, although the majority of AAEM species is retained in the biochars.

Because $PM_{0.1}$ contains dominantly Na, K, and Cl (see Figure 5), further analyses clearly show that the molar ratios of (Na + K)/Cl in samples collected in related different DLPI

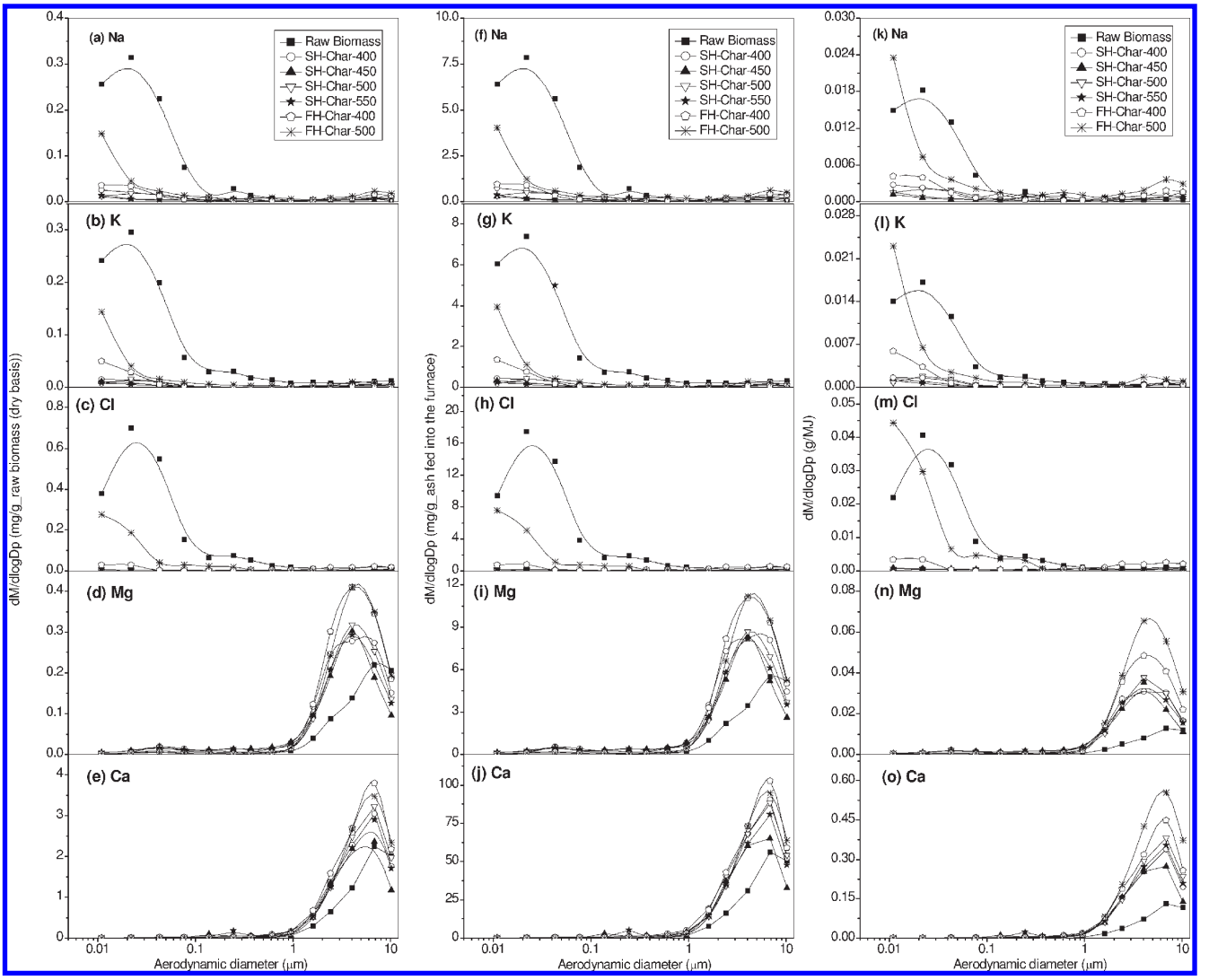

Figure 5. Elemental mass size distribution of AAEM species and Cl in PM during the combustion of raw biomass and biochars: (a) Na, (b) K, (c) Cl, (d) Mg, and (e) Ca are normalized to the equivalent biomass (db) input into the furnace; (f) Na, (g) K, (h) Cl, (i) Mg, and (j) Ca are normalized to the equivalent ash input into the furnace; and (k) Na, (l) K, (m) Cl, (n) Mg, and (o) Ca are normalized to the equivalent energy input (LHV) into the furnace.

stages (that make up $PM_{0.1}$) from raw biomass combustion are all close to 1 (see Figure 7), suggesting that $PM_{0.1}$ generated from raw biomass combustion is mainly composed of alkali (Na and K) chlorides. This also demonstrates the important role of Cl in the formation of ultrafine PM. It is known that Cl is a key element that can substantially enhance the volatilization of alkali metals during biomass pyrolysis.[41] Furthermore, the formation of alkali chloride is also stable under combustion conditions,[48] leading to the subsequent formation of ultrafine PM via either homogeneous nucleation and/or heterogeneous condensation of the alkali chloride vapors on small particles.[22,23,36,46,47] Figure 2 clearly shows that the majority (66.6−98.0%) of Cl was volatilized as part of volatiles during the preparation of biochars even at 400 °C. Therefore, the removal of volatiles during low-temperature pyrolysis of biomass for biochar production leads to not only the lack of the contribution of volatile combustion during biochar combustion but also the lack of Cl in the fuels. This reduces the volatilization of Na and K during biochar combustion, despite the abundant Na and K retained in biochars (see Figure 2). Consequently, the PM_1 yields from biochar combustion are substantially reduced. Such reasoning also seems to be consistent with the higher PM_1 yield during the combustion of fast pyrolysis biochar produced at 500 °C because this char has a substantially higher Cl content.

For PM_{1-10}, it is clearly seen in Figures 3−6 that there are substantial increases in the yields of PM_{1-10}, which dominantly contains Mg and Ca. Particularly, when normalized to equivalent ash input into the furnace (see Figure 4b and panels i and j of Figure 5), the data clearly demonstrate that the contribution of Mg and Ca for PM_{1-10} emission is significantly enhanced during biochar combustion. As already normalized to ash content, the data suggest that such a significant increase must be related to an enhanced char fragmentation during combustion, as a result of changes in the char structure. During char combustion, char fragmentation followed by the release of refractory elements in the burning char is known as a principle mechanism responsible for the formation of PM_{1-10} from both coal and biomass combustion.[22,23,36,46,49,50] Previous investigations showed that the fragmentation of char is strongly dependent upon the char structure.[51,52] An increase in char macroporosity[49] and surface

dx.doi.org/10.1021/ef200296u |*Energy Fuels* 2011, 25, 2702–2710

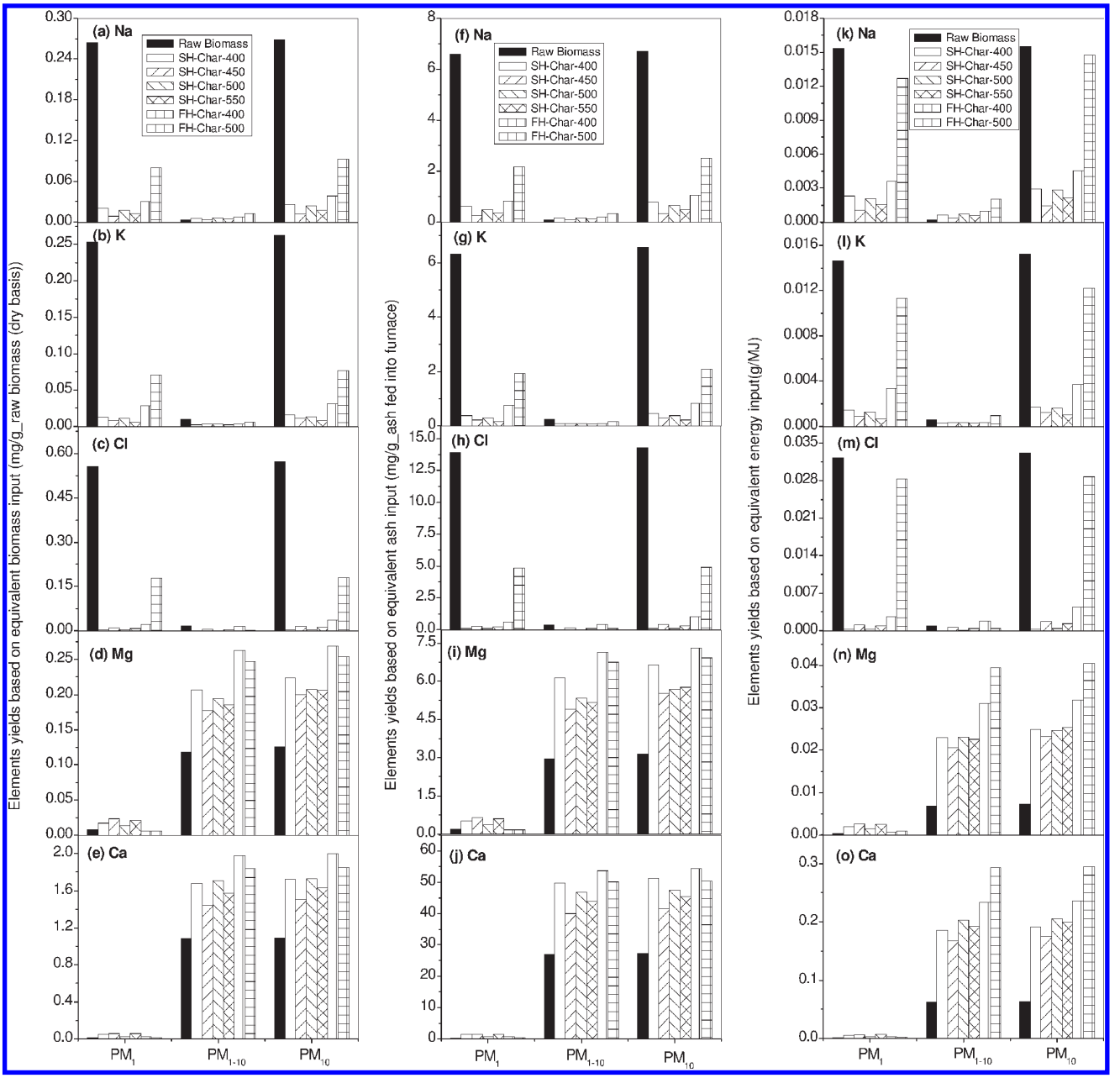

Figure 6. Element yields of AAEM species and Cl in PM during the combustion of raw biomass and biochars: (a) Na, (b) K, (c) Cl, (d) Mg, and (e) Ca, normalized to equivalent biomass (db) input into the furnace; (f) Na, (g) K, (h) Cl, (i) Mg, and (j) Ca, normalized to equivalent ash input into the furnace; and (k) Na, (l) K, (m) Cl, (n) Mg, and (o) Ca, normalized to equivalent energy input (LHV) into the furnace.

area[50] can lead to intensified fragmentation of porous chars. Therefore, further experiments and analysis were then carried out to prepare and characterize the structure of the chars. It should be noted that, because the combustion of biomass and biochars was undertaken at 1300 °C, only the chars prepared from the pyrolysis of the fuels (biomass and biochars) at 1300 °C are relevant, using the same DTF under similar conditions (with argon as a carrier gas instead of air). Indeed, as shown in Figure 8, the micropore surface area of chars produced from biochars is much higher than that from biomass under pyrolysis conditions pertinent to the combustion conditions. Therefore, the substantial increases in the yields of PM_{1-10} during biochar combustion are likely due to the enhanced char fragmentation, resulting from more porous chars from the pyrolysis of biochars under the combustion conditions in comparison to that from biomass.

3.5. Practical Implications. From a practical point of view, it becomes more important to assess the ability of a particular fuel in PM_1 and PM_{10} emissions, normalized to the unit useful energy (LHV) input into the furnace. Such results are presented in panels e and f of Figure 3 (for PM_1 and PM_{10} yield), panels k−o of Figure 6 (for elemental yields in PM_1 and PM_{10}), Figure 4c (for mass-based PSDs), and panels k−o of Figure 5 (for elemental mass-based PSDs). There are three important observations of practical significance that can be made based on the data presented in these figures.

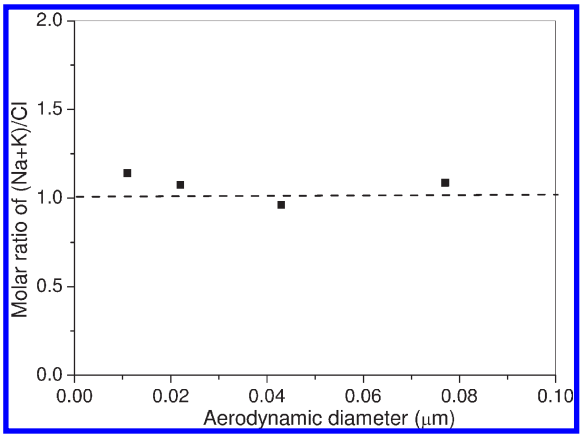

Figure 7. Molar ratio of (Na + K)/Cl in $PM_{0.1}$ collected from raw biomass combustion.

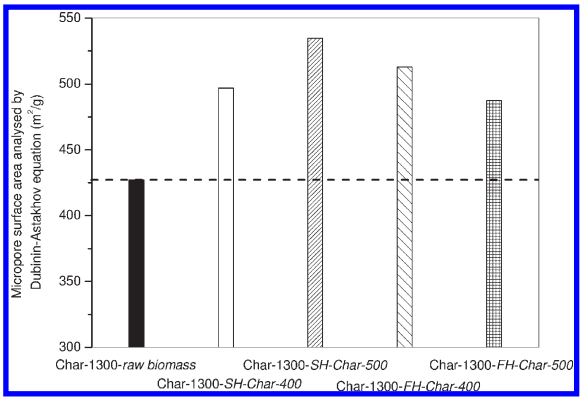

Figure 8. Micropore surface area of biochars produced from the fast pyrolysis of raw biomass, "SH-Char-400", "SH-Char-500", "FH-Char-400", and "FH-Char-500" at 1300 °C in the DTF.

First, per unit energy input, as shown in Figure 3e, the PM_1 yields from biochar combustion may have considerable reductions compared to that from raw biomass combustion. On an elemental basis, as shown in panels k−m of Figure 6, substantial reductions on the yields of Na, K, and Cl in PM_1 are observed. Again, one exception is the fast pyrolysis char prepared at 500 °C that has a high PM_1 yield, possibly related to the high Cl content in the char. Because almost all PM_1 are actually $PM_{0.1}$ (see Figure 4c and panels k−m of Figure 5), the data clearly demonstrate the potential advantage of using biochar as a fuel (via pyrolysis as a fuel pretreatment technology) in effective reduction of sub-micrometer (and ultrafine) PM emission during combustion. This has important practical implications because it is known that PM_1 can easily escape from dust-cleaning equipment.[31,32] Therefore, depending on pyrolysis conditions, biochar as a fuel can potentially offer a simple solution for reducing PM_1 emission during biomass combustion.

Second, during biochar combustion, the substantial reductions in PM_1 yields are however accompanied with substantial increases in PM_{1-10} emission. For example, per an energy input basis, the combustion of "SH-Char-400" and "FH-Char-500" results in increases of PM_{10} yields by 100 and 240% (see Figure 3f), respectively, in comparison to that from biomass combustion. The substantial increases in PM_{10} yields are also reflected in the significant increases in the yields of Mg and Ca in

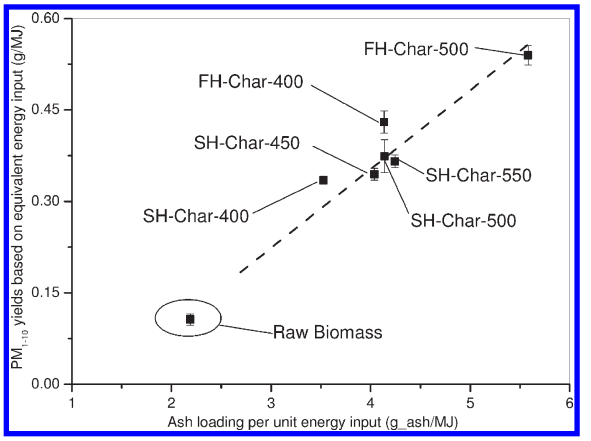

Figure 9. Relationship between the energy-based ash loading of fuels and energy-based yields of PM_{1-10} collected from the combustion of raw biomass and biochars.

PM_{10} (see panels n and o of Figure 6). Therefore, such increases in PM_{1-10} emission during biochar combustion are likely to increase the load of dust-cleaning equipment.

Third, it is also noteworthy that, on an equivalent energy input basis, the mass yields of PM_{1-10} (see Figure 3f) and the yields of dominant elements in PM_{1-10} (Mg and Ca; see panels n and o of Figure 6) during the combustion of different biochars are considerably different. As shown in Figure 8, after pyrolysis at 1300 °C, the selected four biochars, "Char-1300-SH-Char-400", "Char-1300-SH-Char-500", "Char-1300-FH-Char-400", and "Char-1300-FH-Char-500", have similar values of surface area; therefore, the differences in the char structure do not seem to be the reason. A close investigation reveals that different biochars are substantially different in energy-based ash loading, i.e., the amount of ash input into the furnace during combustion normalized to equivalent energy input. The energy-based PM_{1-10} yields during biochar combustion are then plotted against the energy-based ash loading, as presented in Figure 9. A strong correlation between the two is clearly evident. Such reasoning is plausible because more ash inputs would have led to higher PM_{1-10} emissions.

4. CONCLUSION

This paper investigates the emission behavior and characteristics of PM_1 and PM_{10} during the combustion of biomass and its derived biochars [produced from low-temperature pyrolysis at both slow- heating rates (at 400, 450, 500, and 550 °C) and fast-heating rates (at 400 and 500 °C)] using a laboratory-scale DTF system. The major conclusions are drawn as follows: (1) The biochar yields during biomass pyrolysis range from 26.7 to 37.0% depending upon pyrolysis conditions. At such low temperatures, the majority (78.5−100.0%) of AAEM species are retained in biochars after pyrolysis, while the retention of Cl in biochars is only 2.0−33.4%. (2) The PSD of PM_{10} from raw biomass combustion has a bimodal size distribution, ie., a fine mode and a coarse mode. However, the PSDs of PM_{10} from biochar combustion generally shows a unimodal distribution with only a coarse mode, except that of the fast pyrolysis biochar prepared at 500 °C which has a relatively high Cl content. (3) The combustion of biochars leads to substantial reductions in both PM_1 yields and the mass of Na, K, and Cl in PM_1 in comparison

to direct biomass combustion; such reduction is most likely due to the lack of the contribution of volatile (including released inorganic species) combustion to PM_1 formation and the volatilization of Cl during low-temperature pyrolysis of biomass for biochar preparation. (4) Biochar combustion also results in significant increases in the yields of PM_{1-10} and the mass of Mg and Ca in PM_{1-10} compared to those from raw biomass combustion, most likely because of the significant changes in char structures. (5) On the basis of an equivalent energy input into the furnace, there is a strong correlation between the energy-based PM_{1-10} yields and the energy-based ash loading during biochar combustion. An increase in biochar ash loading leads to a significantly increased PM_{1-10} emission.

AUTHOR INFORMATION

Corresponding Author

*Telephone: +61-8-92667592. Fax: +61-8-92662681. E-mail: h.wu@curtin.edu.au.

ACKNOWLEDGMENT

The authors acknowledge the support from Australia Government's International Science Linkage program and the Australian Research Council's Discovery Projects Program. Biomass pyrolysis is also part of a project supported by Australian Government's Second Generation Biofuels Research and Development Grant Program. Xiangpeng Gao is grateful to the EIPRS and CUPS scholarships for his Ph.D. study.

REFERENCES

(1) Bartle, J.; Olsen, G.; Cooper, D.; Hobbs, T. *Int. J. Global Energy Issues* **2007**, *27*, 115–137.
(2) Bartle, J. R.; Abadi, A. *Energy Fuels* **2010**, *24*, 2–9.
(3) Wu, H.; Fu, Q.; Giles, R.; Bartle, J. *Energy Fuels* **2008**, *22*, 190–198.
(4) Yu, Y.; Bartle, J.; Li, C. Z.; Wu, H. *Energy Fuels* **2009**, *23*, 3290–3299.
(5) Yu, Y.; Wu, H. *Energy Fuels* **2010**, *24*, 5660–5668.
(6) Boylan, D. M. *Biomass Bioenergy* **1996**, *10*, 139–147.
(7) Hughes, E. E.; Tillman, D. A. *Fuel Process. Technol.* **1998**, *54*, 127–142.
(8) Prinzing, D. E.; Hunt, E. F. *Fuel Process. Technol.* **1998**, *54*, 143–157.
(9) Moghtaderi, B.; Ness, J. *Australian biomass co-firing handbook,* ISBN 9781921374074, Cooperative Research Centre for Coal in Sustainable Development, 2008.
(10) Zulfiqar, M.; Moghtaderi, B.; Wall, T. F. *Fuel Process. Technol.* **2006**, *87*, 281–288.
(11) Bridgewater, A. V. *Therm. Sci.* **2004**, *8*, 21–49.
(12) Czernik, S.; Bridgewater, A. V. *Energy Fuels* **2004**, *18*, 590–598.
(13) Mohan, D.; Pittman, C. U.; Steele, P. H. *Energy Fuels* **2006**, *20*, 846–889.
(14) Garcia-Perez, M.; Chaala, A.; Pakdel, H.; Kretschmer, D.; Rodrigue, D.; Roy, C. *J. Anal. Appl. Pyrolysis* **2007**, *78*, 104–116.
(15) Mulligan, C. J.; Strezov, L.; Strezov, V. *Energy Fuels* **2010**, *24*, 46–52.
(16) Garcia-Perez, M.; Chaala, A.; Pakdel, H.; Kretschmer, D.; Rodrigue, D.; Roy, C. *Energy Fuels* **2006**, *20*, 364–375.
(17) Garcia-Perez, M.; Wang, X. S.; Shen, J.; Rhodes, M. J.; Tian, F.; Lee, W.; Wu, H.; Li, C. *Ind. Eng. Chem. Res.* **2008**, *47*, 1846–1854.
(18) Abdullah, H.; Wu, H. *Energy Fuels* **2009**, *23*, 4174–4181.
(19) Abdullah, H.; Mediaswanti, K. A.; Wu, H. *Energy Fuels* **2010**, *24*, 1972–1979.
(20) Huber, G. W.; Iborra, S.; Corma, A. *Chem. Rev.* **2006**, *106*, 4044–4098.
(21) Yip, K.; Tian, F.; Hayashi, J.; Wu, H. *Energy Fuels* **2010**, *24*, 173–181.
(22) Christensen, K. A. The formation of submicron particles form the combustion of straw. Ph.D. Dissertation, Technical University of Denmark, Lyngby, Denmark, 1995.
(23) Johansson, L. S.; Tullin, C.; Leckner, B.; Sjövall, P. *Biomass Bioenergy* **2003**, *25*, 435–446.
(24) Seames, W. S. *Fuel Process. Technol.* **2003**, *81*, 109–125.
(25) Strand, M.; Bohgard, M.; Swietlicki, E.; Gharibi, A.; Sanati, M. *Aerosol Sci. Technol.* **2004**, *38*, 757–765.
(26) Boman, C.; Nordin, A.; Boström, D.; Öhman, M. *Energy Fuels* **2004**, *18*, 338–348.
(27) Jimenez, S.; Ballester, J. *Proc. Combust. Inst.* **2005**, *30*, 2965–2972.
(28) Johansson, L. S.; Leckner, B.; Gustavsson, L.; Cooper, D.; Tullin, C.; Potter, A. *Atmos. Environ.* **2004**, *38*, 4183–4195.
(29) Johansson, L. S.; Leckner, B.; Gustavsson, L.; Cooper, D.; Tullin, C.; Potter, A.; Berntsen, M. Particle emissions from residential biofuel boilers and stoves—Old and modern techniques. *Proceedings of the International Workshop "Aerosols in Biomass Combustion"*; Graz, Austria, March 18, 2005; Vol. *6*.
(30) Lind, T.; Kauppinen, E. I.; Hokkinen, J.; Jokiniemi, J. K.; Orjala, M.; Aurela, M.; Hillamo, R. *Energy Fuels* **2005**, *20*, 61–68.
(31) Lind, T.; Valmari, T.; Kauppinen, E. I.; Sfiris, G.; Nilsson, K.; Maenhaut, W. *Environ. Sci. Technol.* **1999**, *33*, 496–502.
(32) Maynard, A. D.; Maynard, R. L. *Atmos. Environ.* **2002**, *36*, 5561–5567.
(33) Encinar, J. M.; Gonzalez, J. F.; Rodriguez, J. J.; Ramiro, M. J. *Fuel* **2001**, *80*, 2025–2036.
(34) Wu, H.; Yip, K.; Tian, F.; Xie, Z.; Li, C.-Z. *Ind. Eng. Chem. Res.* **2009**, *48*, 10431–10438.
(35) Valmari, T.; Lind, T. M.; Kauppinen, E. I.; Sfiris, G.; Nilsson, K.; Maenhaut, W. *Energy Fuels* **1999**, *13*, 379–389.
(36) Lind, T. T.; Valmari, E.; Kauppinen, K.; Nilsson, K.; Sfiris, G.; Maenhaut, W. *Proc. Combust. Inst.* **2000**, *28*, 2287–2295.
(37) Yip, K.; Xu, M.; Li, C.; Jiang, S.; Wu, H. *Energy Fuels* **2011**, *25*, 406–414.
(38) Gao, X.; Wu, H. *Energy Fuels* **2010**, *24*, 4571–4580.
(39) Yip, K.; Wu, H.; Zhang, D.-k. *Energy Fuels* **2007**, *21*, 2883–2891.
(40) Sippula, O.; Lind, T.; Jokiniemi, J. *Fuel* **2008**, *87*, 2425–2436.
(41) Olsson, J. G.; Jäglid, U.; Pettersson, J. B. C.; Hald, P. *Energy Fuels* **1997**, *11*, 779–784.
(42) Quyn, D. M.; Wu, H.; Bhattacharya, S. P.; Li, C. *Fuel* **2002**, *81*, 151–158.
(43) Björkman, E.; Strömberg, B. *Energy Fuels* **1997**, *11*, 1026–1032.
(44) Wang, X.; Si, J.; Tan, H.; Ma, L.; Pourkashanian, M.; Xu, T. *Energy Fuels* **2010**, *24*, 5215–5221.
(45) Quyn, D. M.; Wu, H.; Li, C. Z. *Fuel* **2002**, *81*, 143–149.
(46) Pagels, J. M.; Strand, J. R. *J. Aerosol Sci.* **2003**, *34*, 1043–1059.
(47) Hinds, W. *Aerosol Technology: Properties, Behavior, and Measurement of Airborne Particles*, 2nd ed.; Wiley-Interscience: New York, 1999.
(48) Baxter, L. L.; Miles, T. R.; Dayton, D.; Bryers, R. W.; Oden, L. L. *Fuel Process. Technol.* **1998**, *54*, 47–78.
(49) Helble, J. J.; Sarofim, A. F. *Combust. Flame* **1989**, *76*, 183–196.
(50) Yu, Y.; Xu, M.; Yao, H.; Yu, D.; Qiao, Y.; Sui, J.; Liu, X.; Cao, Q. *Proc. Combust. Inst.* **2007**, *31*, 1947–1954.
(51) Baxter, L. L. *Combust. Flame* **1992**, *90*, 174–184.
(52) Wu, H.; Wall, T.; Liu, G.; Bryant, G. *Energy Fuels* **1999**, *13*, 1197–1202.